Available online at www.sciencedirect.com
ScienceDirect
Trans. Nonferrous Met. Soc. China 25(2015) 2686−2692
Transactions of Nonferrous Metals Society of China
www.tnmsc.cn

Electroplastic effect in AZ31B magnesium alloy sheet through uniaxial tensile tests

Huan-yang XIE[1], Qian WANG[1], Fang PENG[1], Kai LIU[1], Xiang-huai DONG[1], Jian-feng WANG[2]

1. Institute of Forming Technology & Equipment, Shanghai Jiao Tong University, Shanghai 200030, China;
2. General Motor Chinese Science Laboratory Institute, Shanghai 201206, China

Received 24 September 2014; accepted 30 January 2015

Abstract: The electroplastic effect in AZ31B magnesium alloy sheet was investigated through uniaxial tensile tests. In order to show the athermal effect of the electrical pulses, two types of uniaxial tensile tests at the same testing temperature were carried out: uniaxial tension in environmental cabinet and uniaxial tension with electrical pulses. In addition, the distribution of temperature field in the cross-section area during uniaxial tension with electrical pulses was simulated. The results show that the distribution of temperature field along the cross-section area is homogeneous. By comparing the true stress−true strain curves of AZ31B alloy under uniaxial tensile tests, the athermal effect with electrical pulses was confirmed. The microstructure evolution after the uniaxial tension was studied by optical microscopy. The results indicate that the electrical pulses induced dynamic recrystallization plays an important role in the decrease of flow stress. Finally, a flow stress model of AZ31B sheet taking the influence of electroplastic effect into account was proposed and validated. The results demonstrate that the calculated data fit the experimental data well.
Key words: AZ31B magnesium alloy sheet; electroplastic effect; temperature field simulation; microstructure evolution

1 Introduction

When electrical pulses pass through metals undergoing deformation, the flow stress decreases, and the plasticity increases. Such phenomenon is called the electroplastic effect (EPE). EPE has been used in wire drawing [1−3], compression [2], rolling [4−6], bending [7,8], heat treatment [9], etc, and was found very promising in improving formability and surface quality, as well as in springback elimination. However, up to now, the mechanisms of the EPE still remain unclear. Some researchers believed the existence of athermal effect (also called the pure EPE) of the electrical pulses. PERKINS et al [10] carried out compression tests on various metals, such as aluminum alloy and copper alloy, with electrical current and the results indicated that the effect of electrical flow on the materials (i.e., the flow stress reductions) significantly exceeded what can be explained through resistive heating effects. FAN et al [11] investigated the influence of grain size and grain boundaries on the thermal and mechanical behavior of 70/30 brass under electrically-assisted deformation and the results showed that the increased reductions in flow stress were observed in electrically-assisted tension tests rather than in oven-heated thermal tension tests at similar temperatures. XIE et al [12] investigated the influence of the electrical parameters on spingback of AZ31B magnesium alloy and confirmed the existence of the pure EPE. LIU et al [13] also pointed out the existence of pure EPE through uniaxial tension of AZ31B magnesium alloy. However, other researchers considered the EPE as the thermally dominated effect. CONRAD [14] evaluated the effect of the current pulses as a thermally-activated plastic process. MAGARGEE et al [15] investigated the influence of continuous current on the flow stress of commercially pure titanium (CP titanium, Grade 2) sheet and pointed out that no pure EPE was observed and attributed the reduction of flow stress to the thermal softening. KINSEY et al [16] studied the EPE at high deformation rates for 304SS and Ti−6Al−4V subjected Kolsky bar tension deformation and the results showed that the pure EPE did not exist either. GOLDMAN et al [17] indicated that at

Foundation item: Projects (50975174, 51275297) supported by the National Natural Science Foundation of China; Project (20100073110044) supported by the Education Ministry of China
Corresponding author: Xiang-huai DONG; Tel/Fax: +86-21-62813435; E-mail: dongxh@sjtu.edu.cn
DOI: 10.1016/S1003-6326(15)63892-4

temperatures above 20 K, the interaction of electrons and dislocations was negligible and any stress reductions above this temperature must be caused by heating. Thus, whether pure EPE exists or not still remains unclear. It may be a material dependent phenomenon. Recently, based on the free electron theory, LI et al [18] have studied the pure EPE from the microscopic level, but it cannot be easily used to describe the material deformation behavior from the macroscopic level. On the other hand, in theoretical model aspect, models containing the electrical parameters have not been systematically studied, which prevents the application of EPE in electrical pulse-assisted metal forming processes.

In this work, in order to find out whether pure EPE exists or not, two types of uniaxial tensile tests were carried out at the same testing temperature: uniaxial tension in environmental cabinet (isothermal tensile test) and uniaxial tension with electrical pulses. The true stress−strain curves were recorded and compared. In order to understand the temperature distribution along the cross-section area of the sample, coupled thermal-electrical-structure finite element simulation technology was adopted. In order to better understand the mechanism of EPE, the microstructure evolution was studied. Finally, based on the Johnson−Cook model, a flow stress model considering EPE was proposed and validated.

2 Experimental

The experimental material was the commercial cast rolling produced AZ31B magnesium alloy sheet with thickness of 1.5 mm. Its chemical composition is listed in Table 1. The average grain size is 4.6 μm.

Table 1 Chemical composition of as-received AZ31B sheet (mass fraction, %)

Al	Zn	Mn	Fe	Si	Cu	Ni	Mg
2.75	0.64	0.27	0.0023	0.018	0.0016	0.00055	Bal.

The testing samples were cut along the rolling direction to the geometric dimension shown in Fig. 1. The gauge length is 25 mm. All the samples were polished by the abrasive paper to remove the oil and cooling liquid contamination produced during the cutting before the tests.

The testing parameters of tensile test with electrical pulses are listed in Table 2. In Table 2, $\dot{\varepsilon}$ denotes the

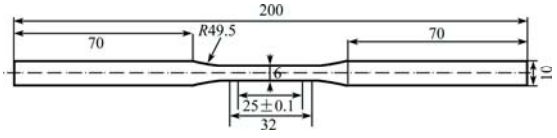

Fig. 1 Dimensions of AZ31B uniaxial tension sample (Unit: mm)

Table 2 Variation of tensile test parameters with electrical pulses

$\dot{\varepsilon}$ /s^{-1}	t/°C	J/(A·mm^{-2})	f/Hz
0.001	100	222.2	120
0.01	150	157.3	240
0.1	200	111.1	480

strain rate (s^{-1}); t denotes the testing temperature (°C); J denotes the peak pulse current density (A/mm^2) and f denotes the pulse frequency (Hz). The temperature distribution on the surface of sample was monitored and recorded by a thermal infrared imager and was controlled by an electric fan. The parameters in the first two columns in Table 2 were employed in uniaxial tensile tests in environmental cabinet. In order to preserve the deformation microstructure, all the samples were put into cold water immediately after tension. In order to ensure the reproducibility, all the experiments were conducted three times.

3 Results and discussion

Before the analysis of the results, the influence of electrical pulses on the temperature distribution should be analyzed firstly. If the temperature field along the cross-section area is homogeneous, the temperature measured by the thermal infrared imager can be considered to be the inside temperature of the sample. Under this circumstance, the difference between the uniaxial tension in environmental cabinet and uniaxial tension with electrical pulses can be considered to be induced by pure EPE. Otherwise, if the temperature inside the sample is quite higher than its surface temperature, the difference between the uniaxial tension in environmental cabinet and uniaxial tension with electrical pulses may be caused by the inside higher temperature which is still considered to be thermal effect.

3.1 Temperature field simulation

During the simulation, coupled thermal−electrical−structural finite element simulation technology is adopted. The sample is uniaxial tensioned to ε=0.01 and the testing temperature is set as 100 °C. In simulation, the material density is 1.78 mg/mm^3, the thermal conductivity is 0.101 W/(mm·°C), the electric conductivity is 9709 S/mm, the specific heat capacity is 1130 J/(kg·°C), the Joule heat fraction is 1, the elastic modulus is 4.18×10^{10} Pa, the poisson ratio is 0.33. The yield stress−plastic strain data are imported from the experimental result at the same testing parameters conducted in the environmental cabinet. The current density is 6.5 A/mm^2, and the initial temperature of the sample is 25 °C. The 8-node brick element (Q3D8H) is

adopted. The heat transfer coefficient is 6.3×10^{-5} W/(mm^2·°C). The time period is 40 s which is the same as the actual situation. The testing temperature keeps at 100 °C with the help of the electric fan. The experimental and simulated results are shown in Fig. 2.

Seven points are selected in the testing sample and the corresponding temperatures of the selected points (sp) are 77.73, 91.25, 100.07, 93.76, 80.46, 35.02 and 35.50 °C, respectively. In simulation, the points in the same position corresponding to Fig. 2(a) are selected for comparison, as shown in Fig. 2(b). The temperature comparison of the selected points is shown in Fig. 3. It indicates that the simulated data fit the experimental data well.

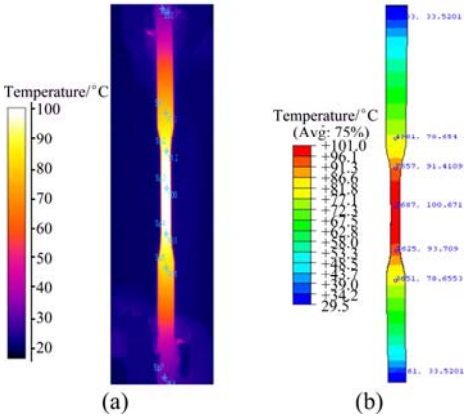

Fig. 2 Temperature field distribution of experimental (a) and simulated (b) results

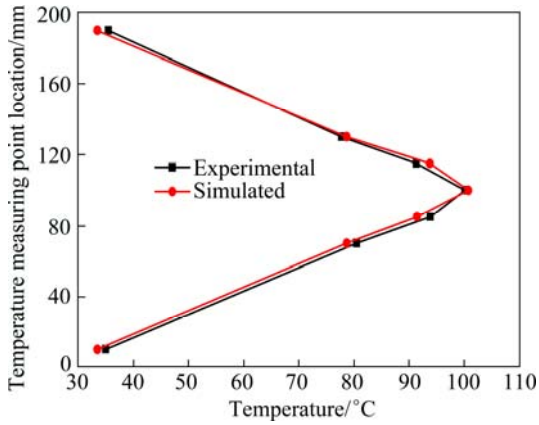

Fig. 3 Comparison between simulated and experimental temperatures

In order to investigate whether temperature gradient along the cross-section area exists or not, temperature distribution on a random cross-section area within the gauge length is studied, as shown in Fig. 4. Thirteen points from the surface of the sample with 0.125 mm increment along the middle line in thickness direction are selected, as shown in Fig. 4(a). The corresponding temperatures at the selected nodes are shown in Fig. 4(b). It can be seen from Fig. 4(b) that the highest temperature along the cross-section area is right in the center of the sample and the temperature difference between the surface and center is 0.005 °C which can be neglected. Therefore, the temperature along the cross-section area can be considered to be homogeneous.

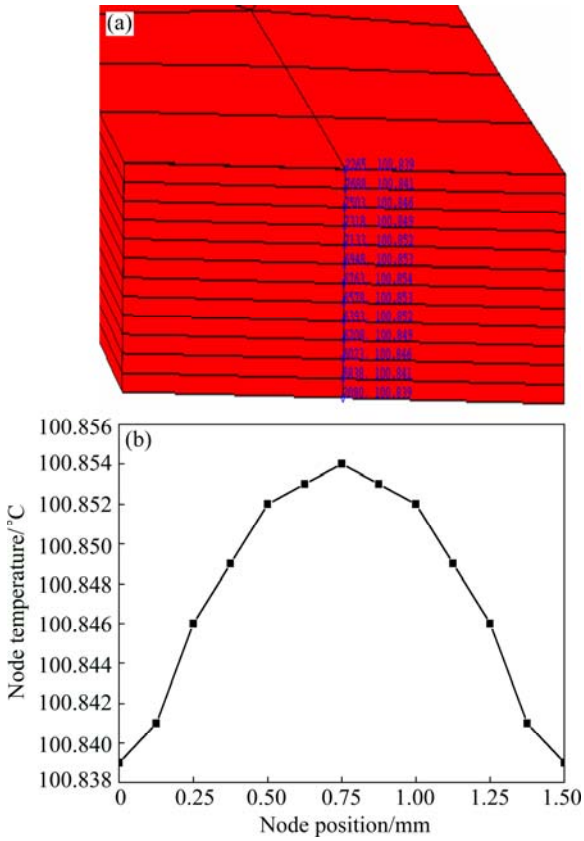

Fig. 4 Selected nodes (a) and corresponding temperature distribution (b) along cross-section area

3.2 Flow behavior

Some selected true stress−true strain curves with error bar are shown in Fig. 5. It can be seen from Fig. 5 that as temperature increases, the flow stress decreases. At the same temperature, the flow stress with electrical pulses is lower than that in isothermal tension without electrical pulses, which means that pure EPE exists in

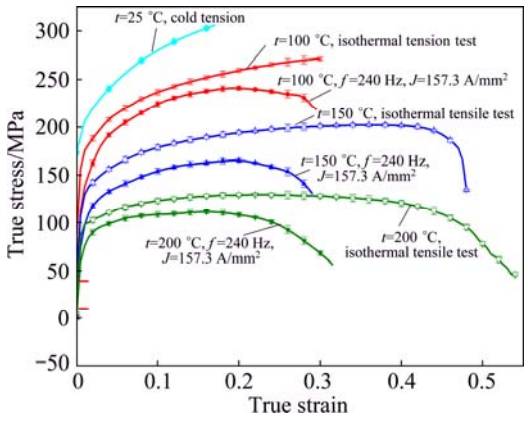

Fig. 5 True stress−true strain curves of AZ31B under uniaxial tensile tests with strain rate of 0.01 s^{-1}

AZ31B. This can be ascribed to the interaction between the drifting electrons and the dislocations. The force exerted on the dislocations can facilitate the movement of dislocation, leading to low external force. The elongation rate increases with increasing the temperature in isothermal tension, but it seems to be not affected by the temperature in tensile tests with electrical pulses. This is because that as the tension progresses, necking occurs and the transient temperature in the necking part is very high, leading to the melting of the material, thus brings about earlier fracture.

3.3 Microstructure evolution

The metallographic photos of tensile samples near necking area are shown in Fig. 6. Comparing Figs. 6(a) with (b), it can be seen that twinning occurs during cold tension, which is the main mechanism of plastic deformation, so the flow stress is higher. When the temperature is 150 °C, dynamic recrystallization (DRX) along the grain boundaries is observed, as shown in Fig. 6(c), which leads to softening. Comparing Figs. 6(c) with (d), it is noticed that the pulse brings about more recrystallized grains. ZHU et al [6] indicated that when rolling with electrical pulses, DRX occurred at a relatively low temperature compared with the traditional hot rolling. STOLYAROV [19] indicated that with the help of the electrical pulses, nanostructure can be easily obtained when rolling TiNi shape-memory alloys with a subsequent annealing. LIU et al [13] pointed out that the electrical pulses could influence the rotation of crystal lattice, and lead to the crystals rotating to a softer orientation, which induced the drastic dynamic softening before necking and decreased the flow stress.

So, it is inferred that the electrical pulses may promote the recrystallization nucleation rate, which contribute to further decrease of flow stress, i.e., pure EPE.

3.4 Flow stress model

Based on the test results, a flow stress model used to describe the homogeneous deformation before necking considering EPE is proposed by modifying the Johnson−Cook model [20]

$$\sigma = (A + B\varepsilon^n)\left[1 + C\ln\left(\frac{\dot{\varepsilon}}{\dot{\varepsilon}_0}\right)\right]\cdot \left[1 - \left(\frac{t - t_r}{t_m - t_r}\right)^m\right]\exp(DJ\sqrt{f}) \quad (1)$$

where EPE is introduced by the last factor, in which D is a material constant, A, B, n, C and m are the parameters similar to Ref. [14], $\dot{\varepsilon}_0$ is the reference strain rate, t_r and t_m are the room and melting temperatures, respectively. The pulse current effective value denoted by I_{ev} can be calculated by

$$I_{ev} = KJ\sqrt{f} \quad (2)$$

where K is a constant and I_{ev} represents the intensity of the pulse current exerted on the material. Increasing I_{ev} will increase the number of drifting electrons in each unit area and the number of pulse current in each unit time, which may facilitate the interaction between drifting

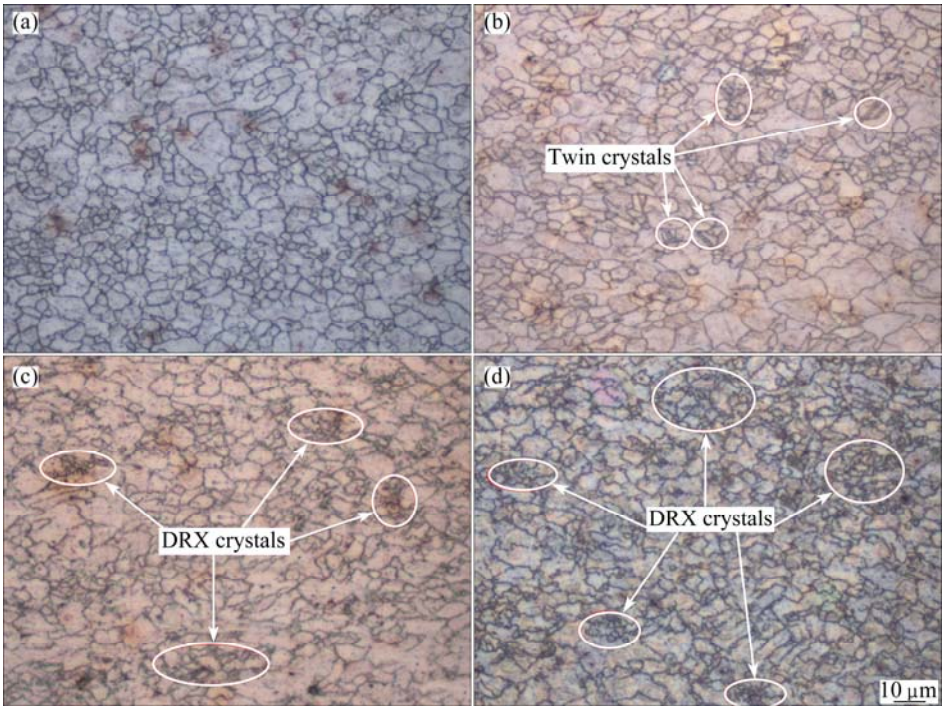

Fig. 6 Metallographic photos of AZ31B tensile samples: (a) Original sample; (b) After cold tension, $\dot{\varepsilon}$=0.01 s^{-1}; (c) After tension without pulse (t=150 °C, $\dot{\varepsilon}$=0.01 s^{-1}); (d) After tension with pulse (t=150 °C, $\dot{\varepsilon}$=0.01 s^{-1}, f=480 Hz, J=157.3 A/mm^2)

electrons and dislocations and help the dislocations move forward. Therefore, I_{ev} is chosen as the influencing parameter of EPE.

All the parameters in the model are determined according to the tensile test results. From the true stress−strain curves without electrical pulses, with $\dot{\varepsilon}=\dot{\varepsilon}_0=0.001\ s^{-1}$ and t=t_r=25 °C, the value of A is determined as A=173.07 MPa. Under such condition, Eq. (1) can be written as

$$\sigma=A+B\varepsilon^n \tag{3}$$

The value of n is determined by the slope of $\ln(\sigma-A)-\ln\varepsilon$ curve as n=0.5, the value of B is determined by the slope of $(\sigma-A)-\varepsilon^n$ curve as B=326.35 MPa.

Other parameters are determined with the Matlab optimization algorithm method. C=0.11, m=0.41, D=−4.36×10^{-5}. Therefore, the flow stress of AZ31B considering EPE is expressed as follows:

$$\sigma=\left(173.07+326.35\varepsilon^{0.5}\right)\left[1+0.11\ln\left(\frac{\dot{\varepsilon}}{\dot{\varepsilon}_0}\right)\right]\cdot\left[1-\left(\frac{t-t_r}{t_m-t_r}\right)^{0.41}\right]\exp\left(-4.36\times10^{-5}J\sqrt{f}\right) \tag{4}$$

The flow stress model suits for 100 °C ≤ t ≤ 200 °C, 0.001 s^{-1} ≤ $\dot{\varepsilon}$ ≤ 0.1 s^{-1}, 120 Hz ≤ f ≤ 480 Hz, 111.1 A/mm^2 ≤ J ≤ 222.2 A/mm^2.

To validate the proposed flow stress model, further EPE-assisted tensile tests are implemented, and the true stress−true strain curves are compared with those predicted by the model shown in Fig. 7. It can be seen from Fig. 7 that the experimental and calculated curves are close to each other. From Fig. 7, it can also be seen that the flow stress σ is mainly affected by the temperature and strain rate, and the effect of pure EPE is of second order.

Another thing is that as the strain increases, the deviation between the calculated and experimental data becomes more evident. The reason is that during tension, the cross-section area of the sample decreases and hence results in higher instantaneous current density which brings even higher testing temperature than the desired. There exists hysteresis phenomenon when controlling the testing temperature with an electric fan. Therefore, the instantaneous high testing temperature induced softening results in even low flow stress.

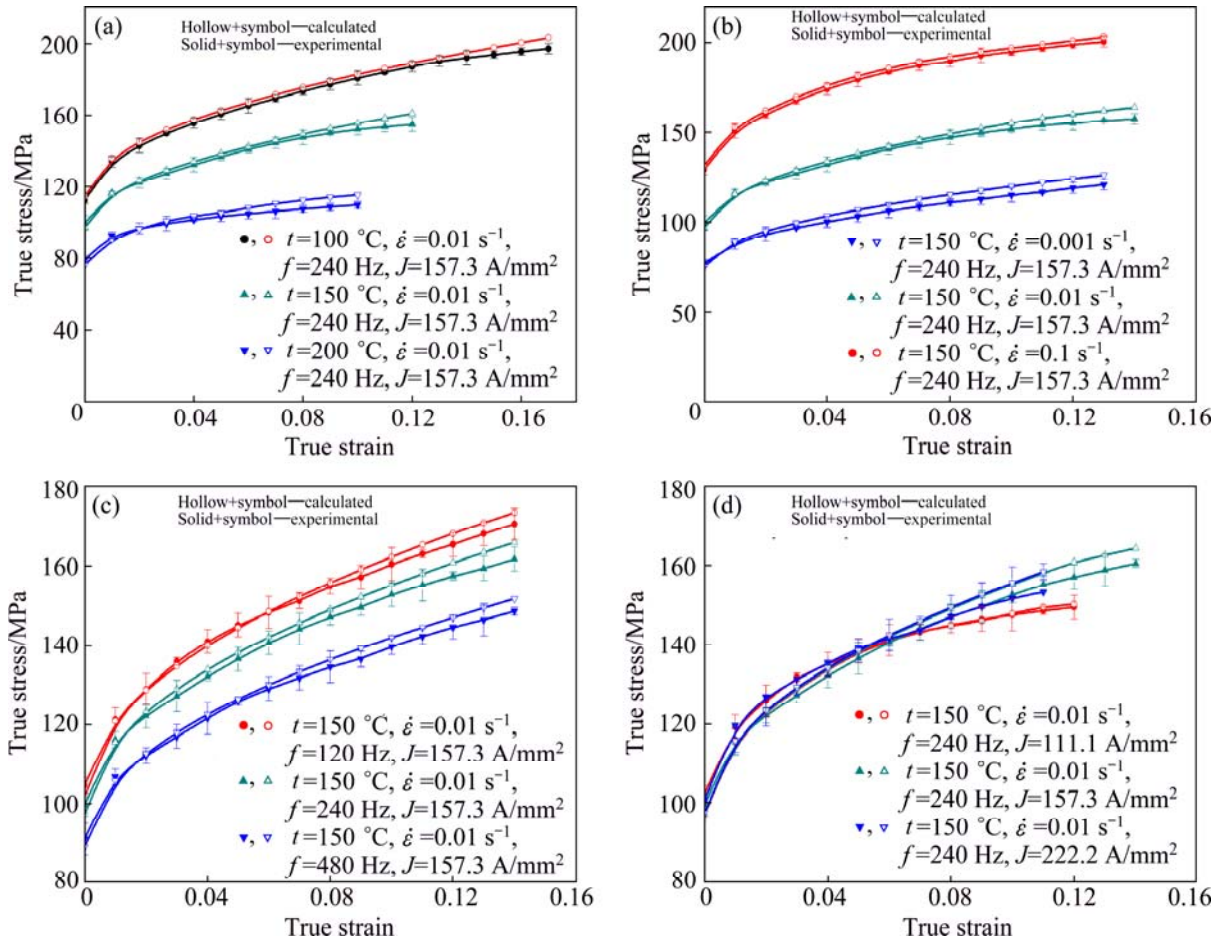

Fig. 7 Comparison of experimental and predicted true stress−true strain curves with varying different parameters: (a) t; (b) $\dot{\varepsilon}$; (c) f; (d) J

4 Conclusions

1) The coupled thermal−electrical−structural finite element simulation technology is adopted to simulate the temperature field along the cross-section area during tension and the result turns out to be homogeneous. This indicates that the monitored temperature on the material surface also represents the temperature inside the material.

2) Comparing the curves with and without electrical pulses at the same temperature, the lower flow stress in tensile tests with electrical pulses can be ascribed to the interaction between the drifting electrons and the dislocations. The force exerted on the dislocations can facilitate the movement of dislocation, leading to low external force. While the low elongation rate in tensile tests with electrical pulses is that as the tension progresses, necking occurs and the transient temperature in the necking part is very high, leading to the melting of the material, thus brings about earlier fracture.

3) Pure EPE is confirmed in AZ31B sheet metal, which promotes dynamic recrystallization nucleation rate, leading to the crystals rotating to a softer orientation, and thus decreases the flow stress and increases the formability.

4) By the modification of Johnson−Cook flow stress model, a new flow stress model of AZ31B sheet considering EPE is proposed and validated based on uniaxial tensile tests (suits for: 100 °C $\leq t \leq$ 200 °C, 0.001 $s^{-1} \leq \dot{\varepsilon} \leq$ 0.1 s^{-1}, 120 Hz $\leq f \leq$ 480 Hz, 111.1 A/mm$^2 \leq J \leq$ 222.2 A/mm^2), which will be adopted in numerical simulation in the future.

References

[1] ZIMNIAK Z, RADKIEWICZ G. The electroplastic effect in the cold-drawing of copper wires for the automotive industry [J]. Archives of Civil and Mechanical Engineering, 2008, 8(2): 173−179.

[2] ROSS C D, IRVIN, D B, ROTH J T. Manufacturing aspects relating to the effects of direct current on the tensile properties of metals [J]. Journal of Engineering Materials and Technology, 2007, 129(2): 342−347.

[3] TANG Guo-yi, ZHANG Jin, YAN Yun-jie, ZHOU Hui-hua, FANG Wei. The engineering application of the electroplastic effect in the cold-drawing of stainless steel wire [J]. Journal of Materials Processing Technology, 2003, 137(1−3): 96−99.

[4] LU Yong-jin, QU Ti-ming, ZENG Pan, LEI Li-ping, FANG Gang, SUN Jian-feng. The influence of electroplastic rolling on the mechanical deformation and phase evolution of Bi-2223/Ag tapes [J]. Journal of Materials Science, 2010, 45(13): 3514−3519.

[5] LIAO Hao-ming, TANG Guo-yi, JIANG Yan-bin, XU Qing, SUN Shi-ding, LIU, Jia-nan. Effect of thermo-electropulsing rolling on mechanical properties and microstructure of AZ31 magnesium alloy [J]. Materials Science and Engineering A, 2011, 529: 138−142.

[6] ZHU Ru-fei, TANG Guo-yi, SHI Sang-qiang, FU Ming-wang. Effect of electroplastic rolling on deformability and oxidation of NiTiNb shape memory alloy [J]. Journal of Materials Processing Technology, 2013, 213(1): 30−35.

[7] GREEN C R, MCNEAL T A, ROTH J T. Springback elimination for Al-6111 alloys using electrically-assisted manufacturing (EAM) [J]. Transactions of the North American Manufacturing Research Institute of SME, 2009, 37: 403−410.

[8] SÁNCHEZ EGEA A J. GONZÁLEZ ROJAS H A, CELENTANO D J, TRAVIESO-RODRÍGUEZ J A, LLUMÀI FUENTES J. Electroplasticity-assisted bottom bending process [J]. Journal of Materials Processing Technology, 2014, 214(11): 2261−2267.

[9] SONG Hui, WANG Zhong-jin, GAO Tie-jun. Effect of high density electropulsing treatment on formability of TC4 titanium alloy sheet [J]. Transactions of Nonferrous Metals Society of China, 2007, 17(1): 87−92.

[10] PERKINS T A, KRONENBERGER T J, ROTH J T. Metallic forging using electrical flow as an alternative to warm/hot working [J]. Journal of Manufacturing Science and Engineering, 2007, 129(1): 84−94.

[11] FAN R, MAGARGEE J, HU P, CAO J. Influence of grain size and grain boundaries on the thermal and mechanical behavior of 70/30 brass under electrically-assisted deformation [J]. Materials Science and Engineering A, 2013, 574: 218−225.

[12] XIE Huan-yang, WANG Qian, LIU Kai, PENG Fang, DONG Xiang-huai, WANG Jian-feng. Investigation of influence of direct-current pulses on springback during V-bending of AZ31B magnesium alloy sheet [J]. Journal of Materials Processing Technology, 2015, 219: 321−327.

[13] LIU K, DONG X, XIE H, PENG F. Effect of pulsed current on the deformation behavior of AZ31B magnesium alloy [J]. Materials Science and Engineering A, 2015, 623: 97−103.

[14] CONRAD H. Thermally activated plastic flow of metals and ceramics with an electric field or current [J]. Materials Science and Engineering A, 2002, 322: 100−107.

[15] MAGARGEE J, MORESTIN F, CAO J. Characterization of flow stress for commercially pure titanium subjected to electrically assisted deformation [J]. Journal of Engineering Materials and Technology, 2013, 135: 0410031.

[16] KINSEY B L, CULLEN G, JORDAN A, MATES S. Investigation of electroplastic effect at high deformation rates for 304SS and Ti−6Al−4V [J]. CIRP Annals Manufacturing Technology, 2013, 62(1): 279−282.

[17] GOLDMAN P D, MOTOWIDLO L R, GALLIGAN J M. The absence of an electroplastic effect in lead at 4.2 K [J]. Scripta Metallurgica, 1981, 15(4): 353−356.

[18] LI Da-long, YU En-lin, LIU Zhou-tong. Mechanism research and progress of metal's pure electroplastic effect [J]. Applied Mechanics and Materials, 2012, 184−185: 1060−1063.

[19] STOLYAROV V V. Deformability and nanostructuring of TiNi shape-memory alloys during electroplastic rolling [J]. Materials Science and Engineering A, 2009, 503(1−2): 18−20.

[20] JOHNSON G R, COOK W H. A constitutive model and data for metals subjected to large strains, high strain-rates and high temperatures [C]//Proceedings of the 7th International Symposium on Ballistics. Hague, Netherlands, 1983: 541−547.

单向拉伸试验研究 AZ31B 镁合金板材的电塑性效应

解焕阳[1]，王 倩[1]，彭 芳[1]，刘 凯[1]，董湘怀[1]，王建峰[2]

1. 上海交通大学 塑性成形技术与装备研究院，上海 200030；
2. 通用汽车中国科研院，上海 201206

摘 要：通过单向拉伸试验研究镁合金 AZ31B 的电塑性效应。为了显示脉冲电流的非热效应，在相同温度下开展两类试验：环境箱中的单向拉伸试验和脉冲电流辅助的单向拉伸试验。此外，对脉冲电流在材料变形过程中引起的温度场进行数值模拟。结果表明，沿材料截面方向温度分布均匀。通过对比两类单向拉伸试验的真应力−真应变曲线，证实了脉冲电流非热效应的存在。通过光学显微镜研究脉冲电流对材料微观组织演化的影响，结果表明：脉冲电流引起的动态再结晶对流动应力的下降起重要作用。最后，提出一个考虑电塑性响应的 AZ31B 流动应力模型，并通过实验进行验证。结果表明：模型预测结果和实验结果吻合较好。

关键词：AZ31B 镁合金板材；电塑性效应；温度场模拟；组织演化

(Edited by Mu-lan QIN)